Title

USE OF THE FOUR-INCH LIQUID HYDROGEN BUBBLE CHAMBER AS A FAST-NEUTRON SPECTROMETER

Authors

Adelson, Harold E.
Bostick, Hoyt A.
Moyer, Burton J.
et al.

Publication Date

1959-01-15

UNIVERSITY OF CALIFORNIA

Ernest O. Lawrence

Radiation Laboratory

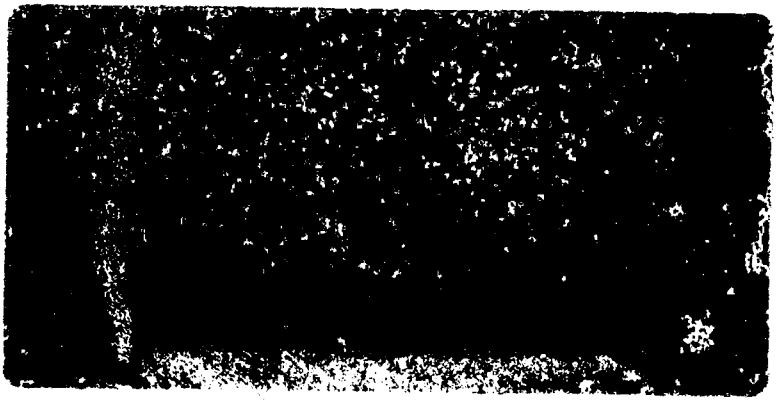

BERKELEY, CALIFORNIA

DISCLAIMER

UCRL-8604

cy 2

UNIVERSITY OF CALIFORNIA
Lawrence Radiation Laboratory
Berkeley, California

Contract No: W-7405-eng-48

USE OF THE FOUR-INCH LIQUID HYDROGEN BUBBLE CHAMBER AS A FAST-NEUTRON SPECTROMETER

Harold E. Adelson, Hoyt A. Bostick, Burton J. Moyer,
and Charles N. Waddell

January 15, 1959

Printed for the U. S. Atomic Energy Commission

USE OF THE FOUR-INCH LIQUID HYDROGEN BUBBLE CHAMBER AS A FAST-NEUTRON SPECTROMETER

Harold E. Adelson, Hoyt A. Bostick, Burton J. Moyer, and Charles N. Waddell

University of California
Lawrence Radiation Laboratory
Berkeley, California

January 15, 1959

ABSTRACT

The 4-inch hydrogen bubble chamber has been used as a neutron spectrometer in the 5- to 30-Mev region. A fast data-reduction system for the analysis of the recoil-proton tracks was developed, utilizing a commercial electronic coordinate-measuring device, the IBM punch-card system, and the IBM 650 digital computer. The resolution of the entire spectrometer system was determined by measuring the monoergic (14.1-Mev) neutron spectrum from the $t(d, n)He^4$ reaction with different neutron collimators. The full width at half maximum of the measured peak was 10% of the peak energy.

USE OF THE FOUR-INCH LIQUID HYDROGEN BUBBLE CHAMBER AS A FAST-NEUTRON SPECTROMETER

Harold E. Adelson, Hoyt A. Bostick, Burton J. Moyer, and Charles N. Waddell

University of California
Lawrence Radiation Laboratory
Berkeley, California

January 15, 1959

I. INTRODUCTION

The absence of an electric charge makes it necessary to detect and measure the energy of neutrons by indirect means. Usually, the neutrons are allowed to interact with a hydrogenous medium, resulting in charged secondaries (protons), which are easier to detect. Descriptions of various measurement techniques have been given in several review articles.[1] In particular, neutrons of energy greater than 1 Mev have been studied by observing recoil protons in neclear emulsions[2] and in cloud chambers;[3] electronic techniques have been successfully applied in the use of recoil counter telescopes[4] and fast time-of-flight systems.[5] There are several desirable characteristics and some disadvantages possessed by both the visual and electronic detection schemes. We report here on efforts to use a hydrogen bubble chamber as a neutron spectrometer.

The development[6] of liquid-hydrogen-filled bubble chambers has made available a device that can serve simultaneously as a source and a detector of recoil protons without contamination by other neutron-induced events. They may be characterized as good-resolution devices without the low detection efficiency encountered in the recoil-proton counter telescope. Although this is also true of hydrogen-filled cloud chambers, there are three significant differences between these two devices. First, the higher

density of protons in liquid hydrogen gives rise to greater neutron-detection efficiency than in a comparable volume of gas. Moreover, because of the reduced recoil-proton track lengths in the liquid, a bubble chamber is suitable for detecting more energetic neutrons than is practical in a hydrogen cloud chamber. Furthermore, a bubble chamber possesses a higher duty cycle than a gaseous cloud chamber, making it possible to gather data more efficiently at a particle accelerator.

It should be noted, however, that the repetition rate of a liquid hydrogen bubble chamber is still low compared with that of most medium-energy accelerators, e.g., the UCRL 31.5-Mev proton linear accelerator[7] maintained a pulse rate of 15 cycles per second while the bubble chamber could be expanded at the rate of only one pulse each 5 seconds. Such a mismatch in duty cycles means that the expected detection-efficiency gain of a bubble chamber over a counter telescope is reduced from the order of a thousand to a factor of about ten.

An important consideration in the application of a bubble chamber to the problems of neutron spectroscopy is the method employed in measuring recoil-proton energies and determining the energies of the associated neutrons. In order to take advantage of the inherent detection efficiency of the bubble chamber, it is necessary to provide analysis of the recoil events that is both rapid and accurate. An electronic coordinate-measuring device with IBM punched-card output and an electronic digital computer were used as the basis of our track-analysis system for the stereo bubble chamber photographs.

The neutrons to be analyzed during the course of this work were produced by the bombardment of several elements with 31.5-Mev protons

from the UCRL proton linear accelerator. It was desired to test the entire neutron-detection system, including environment, shielding, bubble chamber, and the data-analysis system, in situ by producing 14.1-Mev neutrons from low-energy deuteron bombardments of tritium. The origin of these neutrons was made to be the same as that for the targets to be bombarded later by protons.

II. FEATURES OF BUBBLE CHAMBER AND OPERATION

The 4-in.-diameter liquid hydrogen bubble chamber employed in this work has been described previously.[6] A schematic diagram of this chamber is shown in Fig. 1 and a photograph of the glass and steel chamber is given in Fig. 2. The "sensitive" liquid hydrogen occupies a disc-shaped volume that is 4 in. in diameter and 2 in. thick.

A. Photography

The recoil-proton tracks in the liquid hydrogen were photographed by a 35-mm stereo camera located at 90° from the incoming neutron direction. The bubble chamber was illuminated from the rear by light from a xenon-filled flashtube which was focused between the two camera lenses in order to provide dark-field illumination.

Polaroid-Land photographs could be made by using a remotely controlled mirror to place the bubble chamber image before a Polaroid camera which was located at a 90° angle to the stereo camera axis. The rapidly available Polaroid-Land photographs provided convenient checks on chamber operating conditions and track quality.

B. Thermal Control and Track Bias

In order for the neutron-detection device to be effective, it was necessary to insure that background electron tracks arising from the conversion of gamma rays produced in the target be minimized. Since no magnet was used in this work because its heating effect would increase the cycling time of the chamber and would also introduce a large neutron-scattering mass near the chamber, it was necessary to use the method of "track bias" to distinguish between recoil protons and electrons.[6] By operating the chamber at a lower temperature than is normal, it was possible to bias out the minimum-ionizing electrons. However, the chamber could not be allowed to become too cool or the recoil-proton tracks would also begin to disappear. The tolerable temperature variation about the selected operating point of 26°K was ± 0.05°K. This temperature range represented the limits of regulation ability of the 4-in. chamber system, and objectionable electron sensitivity would occasionally appear during the warm portion of a temperature cycle. This effect did not occur during the measurements of neutrons from the d-t reaction because of the absence of gamma-ray production.

C. Collimation and Shielding

A plan view of the experimental arrangement is shown in Fig. 3. A photograph of the bubble chamber in its running position at the linac is given in Fig. 4.

The shielding and beam collimation used for the d-t runs were identical to those used during the succeeding 31.5-Mev proton bombardments and were thus intended to attenuate the gamma-ray background expected in the latter case as well as the scattered neutron background. A 4-in. layer of

lead bricks and a 16-in. layer of borated paraffin were interposed between the beam pipe and the bubble chamber, as can be seen in Fig. 3. The beam was collimated by a pair of 3/4-in. carbon collimators around the strong-focusing magnet set and a pair of 1/2-in. carbon collimators closer to the target chamber. Carbon had been selected for the collimating material because of its high p, n threshold[8] and low neutron-production cross section.[9]

As indicated in Figs. 1 and 2, the 7/8-in.-diameter Mylar entrance window of the bubble chamber was surrounded by a thick steel retaining ring. In order to minimize spectrum distortion because of scattering in the surrounding material, we inserted an iron neutron-collimating assembly between the target and the bubble chamber. This collimator, which can be seen in its running position in Fig. 4, is also shown partially disassembled in Fig. 5. It consisted, in effect, of a 4×6×25-in. block of iron with a 1-in. hole drilled along the length at the center. Brass cylinders 1 in. in diameter, having inner holes of various diameters, could be placed inside the iron in order to test different collimator shapes. The entire collimator was made in slabs for ease in changing the inner collimating hole. The assembly was mounted on a short iron channel with lateral and vertical adjustments.

D. d-t Operation for Resolution Measurement

In order that the neutrons from the d-t reaction should originate at the same place as those expected from the later proton bombardments of selected targets, a tritium-titanium target assembly was located in the target chamber and bombarded by 4-Mev deuterons. These deuterons had been accelerated by the Van de Graaff generator which ordinarily provided the proton beam injection for the linear accelerator. The deuterons

subsequently "coasted" through the unused tank of the linac and were directed by a steering magnet and strong-focusing quadrupole magnet set onto the target (see Fig. 3). The target was composed of tritium absorbed in a titanium disc[10] which was sufficiently thick to stop 2-Mev deuterons. Since the d-t reaction cross section is maximum near a deuteron kinetic energy of 100 kev,[11] it was desired that the deuterons be brought to rest within the tritium-titanium target. A gold foil having a thickness sufficient to reduce the energy of 4-Mev deuterons to less than 2 Mev was placed on the front of the target assembly.

It was found that a beam of deuterons, accelerated by the Van de Graaff generator being pulsed at its usual 15-cps repetition rate, produced a neutron flux in the control room about 70 times the intensity accepted as permissible. Since the bubble chamber repetition rate was only one expansion each 5 seconds, the neutron-flux level was brought within the allowable limit by accelerating deuterons only when the chamber was sensitive. This was done by also applying the trigger pulse for bubble chamber expansion to the deuteron ion source within the Van de Graaff generator, thus obtaining the deuteron beam only when it was effective in the chamber. During initial alignments, when steady beams were required, it was observed that singly ionized hydrogen molecules from the proton source could be made sufficiently abundant to permit the necessary bending- and focusing-magnet adjustments to be made without neutron production. No further adjustment was necessary upon change-over to a deuteron beam, provided the Van de Graaff voltage was held constant. Since deuterons were accelerated only when the bubble chamber was sensitive to radiation, the total charge collected by the target assembly could be used for comparison of various runs. The target holder

was insulated from the target chamber, and a low-leakage condenser and 100% feedback electrometer were connected to measure the collected beam charge. However, no provision was made to insure that electrons could not escape from the target, so that the total collected charge could be considered only as a relative measure of beam intensity. The electrometer output was displayed on two Speedomax recorders to allow indication of beam intensity both to the accelerator operators and to the experimenters.

Collimators of inner diameters of 7/8 in. and 5/8 in. were tested during the d-t measurements as well as the condition without the iron collimating assembly. Background runs were made with the collimator hole closed by a solid brass plug. Data were gathered by running with no target, with a dummy target identical with the real target except for the absence of absorbed tritium, and with the tritium target.

III. ANALYSIS OF DATA

The fundamental relationship for the recoil protons from the collisions of neutrons in an hydrogenous medium is

$$E_p = E_n \cos^2 \theta, \qquad (1)$$

where E_p and E_n are the energies of the recoil proton and incoming neutron respectively, and θ is the angle of recoil with respect to the incident-neutron direction as determined from the target geometry. Therefore, a measurement of the range and angle of the recoil proton would determine the neutron energy. These quantities can be determined from the two-dimensional coordinates of both end points of the track in each stereo view.

However, restrictive conditions were placed on the origin of acceptable recoil protons, since we wished to analyze only those neutrons

which came down the collimator and through the entrance window of the chamber. This necessitated the additional measurement of fixed point in the chamber (a fiducial mark etched on the glass window) in order to establish the absolute position of any track origin.

A. Reading Equipment and Procedure

The device selected for making track measurements was a commercial unit called the OSCAR, Model N-2,* designed for the examination of photographic records of oscilloscope traces. This instrument was basically a 20-inch-square glass projection screen equipped with adjustable perpendicular cursors mechanically connected to two coded-disc type digitizers, one for x and the other for y coordinates. Each digitizer had a four-digit range in which the last digit corresponded to a distance of 0.05 mm on the projection glass. Readout of the coordinates of a point on the screen was accomplished simply by adjusting the cursors so that their intersection lay over the desired point and pushing a foot switch.

For use with the bubble chamber, the OSCAR had to be adapted to stereo projection. We used a common home stereo projector extensively modified so that it could project the nonstandard stereo pairs, which were separated by 3.5 in. on the 35-mm roll film. This projector was further modified by having individual solenoid-operated shutters placed in front of each lens and by having the lenses mounted so that they could be moved both vertically and horizontally with respect to each other. A remotely controlled film-advance system was also added. All these controls and a focus control were located above the projection screen.

*Manufactured by the Benson-Lehner Corporation, Los Angeles, California.

Since the reading procedure was standardized, a shutter-control chassis was given the function of displaying the proper stereo view on the screen at each state of a measurement. The reader, after entering an identification number manually, had only to place the cross hairs at the proper position and press a button for automatic recording of the data. After a measurement, views changed automatically. The reader measured a fiducial position in each view for each picture in order to establish an absolute coordinate system for the tracks in that picture. This IBM "fiducial" card, which recorded the reading for the fiducial marks, was followed by a "track" card for each track in that picture. The track card contained the coordinates of the end points of the track in each view. With this system, shown in Fig. 6, a reader could measure a track in less than 10 seconds.

B. IBM 650 Computations

The new "fiducial card" and the "track cards" formed the data input to the IBM 650 digital computer, which calculated the following quantities for each acceptable track:

l = length of recoil proton track, in cm,

E_p = corresponding proton energy,

θ = polar angle of track with respect to assumed neutron direction,

ϕ = azimuthal angle of track,

E_n = energy of incident neutron,

d = absolute Y coordinate of beginning of track in bubble chamber.

This calculation was made on the basis of a reconstruction of the real-space coordinates of a track from the stereo views. This reconstruction resulted in an apparent depth for a point in the chamber which differed from

the actual depth because of the refractive effects of the liquid-hydrogen–glass–air boundaries. Because we were interested in a small region of the chamber, we assumed that the actual depth was proportional to the apparent depth and determined the constant of proportionality by measuring a known point in the chamber. As a test of the optical reconstruction, imaginary tracks that began and ended at various fiducial marks on the glass walls were measured. A comparison of the known values of the lengths and angles of these tracks with the measured values indicated agreement to better than 1%.

For determining the proton energy corresponding to a given recoil length, a range-energy relationship for protons in liquid hydrogen was developed from the data of Aron et al.[12] by using a value of 0.059 g/cm^3 for the density of super-heated liquid hydrogen at 26°K.[13] The relationship was expressed in the form

$$\ell = a E_p^{\,x}, \qquad (2)$$

where $a = .0126$,

$x = 1.84$,

ℓ = range of protons in centimeters,

E_p = energy of proton in Mev.

In liquid hydrogen, a 10-Mev proton travels approximately 0.9 cm.

The six quantities calculated by the IBM 650 were punched onto an IBM "answer card" which also contained the individual track's identification number. Since there was a complete description of each event on these answer cards, it was easy to obtain any spectral information about the above six quantities by using the IBM 650. The final neutron-energy spectra--in which efficiency corrections were applied--as well as angular distributions were computed in this manner.

C. Acceptability Criteria

It has already been indicated that only tracks that entered the chamber through the 7/8-in.-diameter entrance window would be considered in the final spectra. Figure 7 shows a sketch of the chamber and indicates the "sensitive volume" cylinder. The length of cylinder was determined by consideration of the region of good illumination in both views. For a track to be acceptable, it had to begin within the sensitive-volume cylinder. For this reason, tracks 1 and 2 in Fig. 7 would have been rejected. In the recoil-proton analysis program, such a track would have had no answer card calculated for it. On the other hand, a track must also have ended before the plane KL so that we may be sure it stopped within the chamber. Thus track 3 would have been rejected even though it began within the sensitive volume. Although this track would have had an answer card computed, the card would have had a rejection code number added after its identification number to indicate the reason for its rejection. Track 4 would have been accepted since it started within the sensitive volume and ended before line KL. Track 4 would have been rejected, however, if the angle θ were greater than 30° (the choice of 30° as the angular acceptance limit is explained in Section IV). Its answer card would then contain a specific rejection code number. Thus any track which began in the sensitive volume had an answer card computed for it, but answer cards representing rejected tracks had a code number punched on them. Hence, in the final selection of tracks for the compilation of energy spectra, it was easy to sort out the rejected tracks.

Since it was not possible for the reader to determine when a recoil proton track lay inside the allowed cylindrical volume, all tracks observed

to be in the central portion of the chamber were measured. The IBM computer performed the final selection or rejection of tracks. Approximately one out of every five tracks originally measured was accepted by the analysis program.

D. Instrumental Efficiency Correction

In calculating the efficiency it is necessary to take into account the variation of the n-p cross section with energy, the decrease of the neutron flux in passage through the hydrogen, the angular acceptance limits of 0° to 30°, and the loss of recoils that, even though they start in the sensitive volume, end beyond its limits.

The variation of the n-p cross section is well known and goes approximately as $1/E$ with energy; n-p cross-section data were taken from the curves of Hughes and Harvey for this calculation.[14] The angular distribution of the recoils in the chamber is approximately $\sin 2\theta$, which means that one-fourth of all the recoils lie between 0° and 30°. Above 10 Mev, the angular distribution of the recoils in the center-of-mass system becomes increasingly nonisotropic. A semiempirical formula constructed by Gammel[15] was used to describe the distribution. This formula for the laboratory-system distribution is

$$\sigma(\theta, E_n) = \sigma_T(E_n) \sin 2\theta \left\{ \frac{1 + 2\left(\frac{E_n}{90}\right)^2 \cos^2 2\theta}{1 + {}^2/_3 \left(E_n/90\right)^2} \right\} ; \qquad (3)$$

$\sigma_T(E_n)$ is the total n-p scattering cross section. The factor in parenthesis is a correction to the usual expression for low-energy differential scattering. The effect of the anisotropy of the center-of-mass system distribution upon the fraction of recoils between 0° and 30° as compared to that for isotropy is small, being only a 4% increase at 25 Mev.

The calculation of the absolute efficiency of the bubble chamber as a function of neutron energy was made by considering the sensitive volume to be divided into two sections as shown in Fig. 8. Section 2 was chosen to have length $R(0°, E_n)$ equal to the range of a forward-going proton which has an energy E_n. Thus, Section 1 has a length L-R such that any recoil that begins in this section ends before the end of the chamber (plane KL). Recoils in Section 2, however, may extend beyond the end boundary if their angle is less than some angle θ_{min} which is a function of position in Section 2. The length of Section 2 becomes about 25% of the entire length of the chamber (7.20 cm) at 15 Mev, and above this energy the decrease of efficiency because of the loss of recoils beyond the end boundary of the cylinder is appreciable.

If N_0 is the number of neutrons with energies between E_n and $E_n + dE_n$ incident upon the face of the cylinder, the number of n-p collisions resulting in proton recoils in Section 1 is

$$N_0(E_n) \left[1 - \exp\left\{\frac{-L+R}{\lambda(E_n)}\right\}\right] ,$$

where $\lambda(E_n)$ is the collision mean free path for neutrons of energy E_n. However, only the fraction

$$F_{30}(E_n) = \int_0^{30} \sigma(\theta, E_n)\, d\theta \Big/ \int_0^{90} \sigma(\theta, E_n)\, d\theta$$

of the recoils will be accepted for the spectra. Hence the number N_1, of acceptable recoils produced in Section 1 is given by

$$N_1 = N_0 \left[1 - \exp\left\{\frac{-L+R}{\lambda(E_n)}\right\}\right] F_{30} . \qquad (4)$$

For Section 2 we must consider not only the probability of the formation of a recoil proton and the rejection of recoils at angles greater than 30°, but also the additional loss of tracks because of extension beyond the end of the chamber. A convenient coordinate system for Section 2 is that shown in Fig. 8B, where a distance r is measured from the end of the section. A recoil track produced within an element of length dr at r will extend beyond the end of Section 2 unless it is at an angle θ greater than a certain value θ_{min} with the incoming neutron direction along the cylinder axis. Let R be the range of a proton with $E_n(\theta = 0^0)$ and ℓ be the range of a proton moving at an angle θ_{min} with energy $E_p = E_n \cos^2\theta_{min}$. Then, using Eqs. (1) and (2), we have

$$R = a\, E_n^x \quad \text{and} \quad \ell = a\, E_n^x \cos^{2x}\theta_{min}.$$

Since the projection of ℓ along r is

$$r = \ell \cos\theta_{min},$$

it follows that the relationship determining θ_{min} is

$$\theta_{min} = \cos^{-1}(r/R)^{[1/(2x+1)]}.$$

Since the track will also be rejected if its angle is greater than 30°, it is necessary to find the fraction $F_{30}(r, E_n)$ of recoils generated in dr at r that will lie between $\theta_{min}(r)$ and 30°. This is given by

$$F_{30}(r, E_n) = \int_{\theta_{min}}^{30^{\circ}} \sigma(\theta, E_n)d\theta \Big/ \int_{0^{\circ}}^{90^{\circ}} \sigma(\theta, E_n)d\theta.$$

The number of acceptable recoils generated in dr is therefore

$$N_0 \exp\left\{\frac{-L+r}{\lambda(E_n)}\right\} F_{30}(r, E_n) \frac{dr}{\lambda(E_n)}.$$

The total number N_2 of acceptable recoils generated in Section 2 is then

$$N_2(E_n) = N_0/\lambda(E_n) \int_{r_{min}}^{R(E_n)} \exp\left\{\frac{-L+r}{\lambda(E_n)}\right\} F_{30}(r, E_n)\, dr. \qquad (5)$$

The lower limit of r_{min} is used instead of zero because at $r = r_{min}$, $\theta_{min} = 30^\circ$. Hence from $r = 0$ to $r = r_{min}$ no acceptable tracks are produced, as is shown in Fig. 8C. The determining condition for r_{min} is

$$r_{min} = R\,(\cos 30^\circ)^{(2x+1)}.$$

The total number of acceptable recoils produced in the sensitive-volume cylinder from N_0 neutrons of energy E_n impinging upon it is given by

$$N(E_n) = N_1(E_n) + N_2(E_n). \qquad (6)$$

The absolute efficiency $\epsilon(E_n)$ of the bubble chamber for detecting neutrons of energy E_n is

$$\epsilon(E_n) = \frac{N(E_n)}{N_0(E_n)} = \left[1 - \exp\left\{\frac{-L+R}{\lambda(E_n)}\right\}\right] F_{30}(E_n) + \exp\left\{\frac{-L/\lambda(E_n)}{\lambda(E_n)}\right\} \int_{r_{min}}^{R(E_n)} \exp\left\{r/\lambda(E_n)\right\} F_{30}(r, E_n)\, dr. \qquad (7)$$

The integral was evaluated by expanding the exponential into a power series (four terms was sufficient) and integrating each term. If one neglects the exponential decrease of the flux in Section 2 in this calculation the integration may be easily carried out and the result is in error by 2% at 25 Mev and less at lower energies. The efficiency factor ϵ was evaluated as a function of neutron energy, and the observed energy spectra were corrected by a

factor of $1/\epsilon(E_n)$ in order to get the source spectra. Figure 9 is a plot of the absolute efficiency versus neutron energy for the detection of neutrons by the 4-in. bubble chamber as it was used in this experiment. The curve has roughly a 1/E dependence, but departs from this above 15 Mev because of the loss of tracks beyond the end of the sensitive volume.

IV. d-t SPECTRUM AND RESOLUTION

Measurements of the d-t neutron-energy spectrum were made with the collimators and the bubble chamber at 90° to the direction of the incident deuteron beam. At this angle a spectrum consisting of virtually monoergic neutrons of 14.1-Mev energy is expected.[9] Figures 10, 11 and 12 show the results for the 7/8-in. collimator, 5/8-in. collimator, and no collimator, respectively. The results for each condition are summarized in Table I.

Table I

Effects of collimation on d-t spectrum

Collimator	Full width at half maximum (Mev)	% of total spectrum below 12 Mev
7/8-in. -diam.	1.3	9%
5/8-in. -diam.	1.5	13%
None	1.8	24%

Although the width of the peak when no collimator was used is not much worse than that with collimation, the low-energy tail is substantially increased. The 5/8-in. collimator with its 1.5-Mev full width at half maximum was chosen for taking data during the proton bombardment of the targets. Because of the large amount of iron surrounding the 7/8-in. Mylar

entrance window on the chamber, it was decided to accept recoils that occurred from neutrons entering the chamber through this window only, i.e., recoils beginning in a central cylinder 7/8 in. in diameter. The film reader in scanning the film, however, could not determine visually the depth of a recoil track and recorded all tracks in a region having a cross section of 2 by 1-1/2 in. The 5/8-in. collimator allowed less neutrons into the unacceptable region than did the 7/8-in. collimator, so that reading time for a given number of accepted tracks was reduced by about 30% by use of the smaller collimator.

The spectra shown for these collimators were derived from the acceptance of recoils at angles no greater than 30°. The full width was about twice as large for acceptance of angles up to 45°. This was because a given error in the determination of the recoil angle causes a larger error in the calculation of the incident neutron energy for larger recoil angles, since $dE_n/E_n = 2 \tan \theta d\theta$. Data for the portion from 30° to 45° in comparison to the 0°-to-30° spectrum for the 5/8-in. collimator are shown in Fig. 13. In order to retain good resolution and also to maximize the target-to-background ratio of neutrons in the accepted spectrum, it was decided to accept recoils from 0° to 30° only in proton bombardments.

As shown in Fig. 11, the full width at half maximum for the 5/8-in. collimator was 1.5 Mev. If one calculates the expected spectrum due to 2.0-Mev deuterons stopping in the tritiated-titanium target in the absence of multiple scattering, the spectrum, shown in Fig. 14 Curve A, would have a full width of less than 0.1 Mev. However, the energy of the outgoing neutron in the d-t reaction depends upon the angle the neutrons make with respect to the incident-deuteron direction. Multiple scattering of the

incident deuteron can drastically change this angle from 90° and hence lead to an appreciably wider peak. The projection of the scattering angle on the plane formed by the beam line and bubble chamber axis determines the distortion of the neutron spectrum. The root mean square of the projected scattering angle, $\sqrt{\overline{\theta_p^2}}$, of the deuterons emerging from the gold foil in which they were degraded in energy from 4 Mev to 2 Mev was 10°. By the time the deuteron was degraded in the tritium-titanium foil down to 0.1 Mev, at which energy the d-t interaction has its maximum cross section, $(\overline{\theta_p^2})^{1/2}$ was 17.5°. A computation including multiple-scattering effects yields the spectrum, shown in Fig. 14, Curve B, with a full width of 0.6 Mev.

If one assumes that the source spectrum (0.6 Mev full width), the measured spectrum (1.5 Mev full width) and the resolution function of the complete system (including the reading system)all have Gaussian shapes, then the full width at half maximum of the resolution function is given by

$$R_{\frac{1}{2}} = \left[(1.5)^2 - (0.6)^2 \right]^{1/2}$$

$$= 1.37 \text{ Mev.}$$

Therefore, the resolution of the complete system at 14 Mev was about 10%. There are several factors that contribute to this resolution. There are errors in reading that arise from not placing the cross hairs exactly on the proper bubble image. Tests were conducted in which readers read and reread the same data, without knowing that they were being examined. It was found that a mean error no larger than 0.3 Mev could be attributed to carelessness in reading track and points. Another factor that might contribute to the resolution is the approximation for refraction made in our optical-analysis scheme. However, tests made by measuring between

fiducial marks of the bubble chamber indicate that the method yielded measurements of angles and lengths within 1% of the true value. Other small factors might be the uncertainty, because of target size, in the direction of a neutron from the target, and a variation in sensitivity of the bubble chamber because of too low a temperature, resulting in missing bubbles along a track. This latter effect would cause an unsymmetrical spectrum shifted to the low side, which is not observed in the d-t work. Probably the largest contribution to the resolution occurs from distortion of the source spectrum by the collimator. Neutrons recoiling from the inner "surface" of the collimating hole may enter the bubble chamber with their angles only slightly changed. This would result in a symmetrical distortion of the spectrum and would also explain the better resolution obtained with the larger (7/8-in.-diameter) collimator.

CONCLUSION

The hydrogen bubble chamber, when coupled to a fast data-processing system, appears to be a useful neutron spectrometer with moderately good resolution and high efficiency. Its usefulness will be enhanced when it is utilized with particle accelerators whose duty cycles are more comparable to that of the bubble chamber. It should be noted that the 4-in. chamber was not designed for the purpose of neutron spectroscopy, but was actually a prototype instrument built for testing experimental features to be used in the larger bubble chambers. An instrument designed with neutron measurements in mind should have better temperature regulation and stability, less material in the immediate vicinity of the liquid hydrogen, and--if possible--a 90° stero angle for the camera in order to obtain a more

accurate reconstruction of the tracks in real space. Electronic instruments for data reduction are being developed at this laboratory which, for problems as simple as recoil-proton analysis, could obviate the need for a human reader. These systems should be able to read and analyze a stereo pair of photographs faster than the bubble chamber can go through an expansion cycle.

ACKNOWLEDGMENT

The experiment could not have been accomplished without the aid of the Bubble Chamber Group under the direction of Professor Luis W. Alvarez; in particular, Mr. Arnold Schwemin made several modifications of the chamber which made it suitable for use as a neutron spectrometer. The authors would also like to acknowledge the work of Mr. Arthur W. Barnes, who designed and maintained much of the data-analysis equipment.

This work was done under the auspices of the U. S. Atomic Energy Commission.

References

1. Barschall, Rosen, Taschek, and Williams, Revs. Modern Phys. 24, 1 (1952); B. T. Feld, The Neutron, in Experimental Nuclear Physics, E. Segrè, Ed. (Wiley, New York, 1953); A. Wattenberg, The Standardization of Neutron Measurements, Annual Review of Nuclear Science 3, 119 (1953).
2. J. Rotblat, Photographic Emulsion Technique, in Prog. in Nuclear Phys. 1, 37 (1950); E. R Graves and L. Rosen, Phys. Rev. 89, 343 (1953).
3. C. Y. Chih and W. M. Powell, Phys. Rev. 106, 539 (1957).
4. C. H. Johnson and C. C. Trail, Rev. Sci. Instr. 27, 468 (1950); R. L. Ribe and J. D. Seagrave, Phys. Rev. 94, 934 (1954); see also Reference 15.
5. L. Cranberg and J. S. Levin, Phys. Rev. 103, 343 (1956); Weber, Johnstone, and Cranberg, Rev. Sci. Instr. 27, 166 (1956).
6. D. Parmentier and Schwemin, Rev. Sci. Instr. 26, 954 (1955); H. C. Dittler and T. F. Gerecke, Liquid Hydrogen Bubble Chambers (M. S. thesis), UCRL-2985, May 1955 (unpublished).
7. This proton linear accelerator is now at the University of Southern California.
8. F. Ajzenberg and T. Lauritsen, Revs. Modern Phys. 27, 77 (1955).
9. Tai, Millburn, Kaplan, and Moyer, Phys. Rev. 109, 2086 (1958).
10. The tritium-titanium target was prepared by and kindly loaned to us by Mr. Jack K. Hum of Lawrence Radiation Laboratory, Livermore.
11. J. L. Fowler and J. E. Brolley, Jr., Revs. Modern Phys. 28, 117 (1956).

12. Aron, Hoffman, and Williams, Range-Energy Curves, AECU-663, 1949.

13. D. Chelton and D. Mann, Cryogenic Data Book, UCRL-3421.

14. D. J. Hughes and J. A. Harvey, Neutron Cross Sections, BNL-325, July 1955.

15. Bame, Haddad, Perry, and Smith, Rev. Sci. Instr. 28, 997 (1957).

Figure Captions

Fig. 1. Schematic vertical section of the 4-in. hydrogen bubble chamber.

Fig. 2. Four-in.-diameter hydrogen bubble chamber.

Fig. 3. Schematic diagram of the acceleration system used to produce a 4-Mev deuteron beam at the target position. The shielding and beam collimation were identical to that utilized for the 31.5-Mev proton bombardment.

Fig. 4. Four-inch liquid hydrogen bubble chamber, neutron collimator, and target chamber in bombardment position at the UCRL proton linear accelerator. (Some of the shielding around the exit beam pipe on the right has been removed to show the target chamber.)

Fig. 5. The iron neutron collimator shown partially disassembled. The central replaceable collimating cylinder and the jacks for horizontal and vertical alignment can be seen.

Fig. 6. The IBM card punch, OSCAR film reader, and projection control unit used for recoil-track measurements.

Fig. 7. Schematic diagram of the 4-in. hydrogen bubble chamber, showing the acceptable volume for recoil proton tracks. Track examples 1, 2, and 3 would be rejected in the analysis program while track 4 would be accepted only if angle θ were less than 30°.

Fig. 8. Diagrams of the division of the acceptable "sensitive volume" of the bubble chamber into two sections for a given neutron energy E_n for the calculation of the efficiency. Section 1 is the region of complete recoil-track containment, whereas Section 2 allows loss of forward-going tracks because of extension beyond the end of the cylinder.

Fig. 9. Absolute efficiency for neutron detection of the 4-in. hydrogen bubble chamber as it was used in this experiment.

Fig. 10. Measured energy spectrum of neutrons from the $t(d, n)He^4$ reaction observed at 90° with the 7/8-in.-diameter collimator.

Fig. 11. Measured energy spectrum of neutrons from the $t(d, n)He^4$ reaction observed at 90° with the 5/8-in.-diameter collimator.

Fig. 12. Measured energy spectrum of neutrons from the $t(d, n)\ He^4$ reaction observed at 90° without the neutron collimator.

Fig. 13. Comparison of the measured neutron spectra from the $t(d, n)He^4$ reaction at 90° with the 5/8-in. collimator, obtained by accepting 0°-to-30° recoil protons and 30°-to-45° recoil protons.

Fig. 14. Curve A is the calculated neutron spectrum at 90° if no multiple scattering of the deuterons occurred. The full width at half maximum is less than 0.1 Mev. Curve B shows the effect of multiple scattering of the deuterons in the gold foil and the tritium-titanium target. The full width at half maximum is 0.6 Mev.

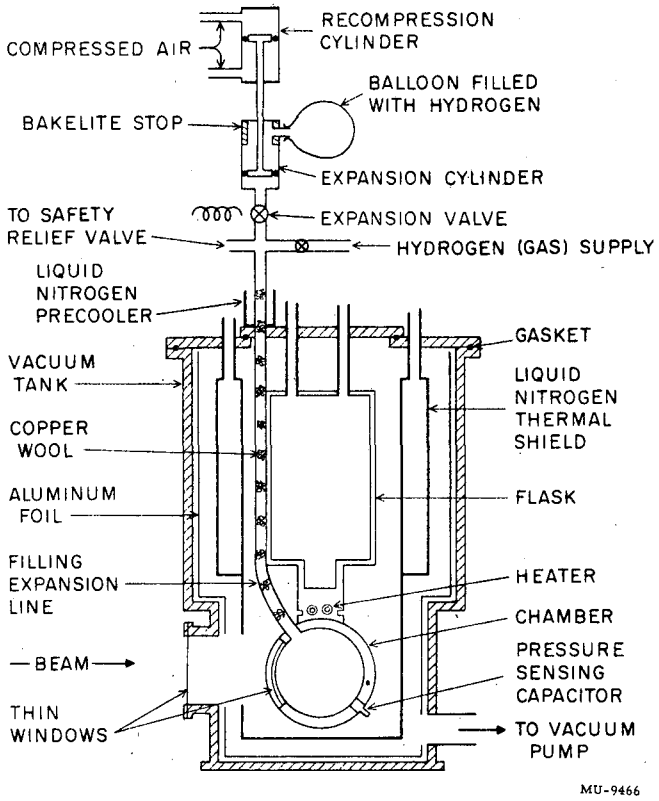
COMPRESSED AIR
RECOMPRESSION CYLINDER
BALLOON FILLED WITH HYDROGEN
BAKELITE STOP
EXPANSION CYLINDER
TO SAFETY RELIEF VALVE
EXPANSION VALVE
HYDROGEN (GAS) SUPPLY
LIQUID NITROGEN PRECOOLER
GASKET
VACUUM TANK
LIQUID NITROGEN THERMAL SHIELD
COPPER WOOL
ALUMINUM FOIL
FLASK
FILLING EXPANSION LINE
HEATER
CHAMBER
BEAM
PRESSURE SENSING CAPACITOR
THIN WINDOWS
TO VACUUM PUMP
MU-9466

Fig. 1.

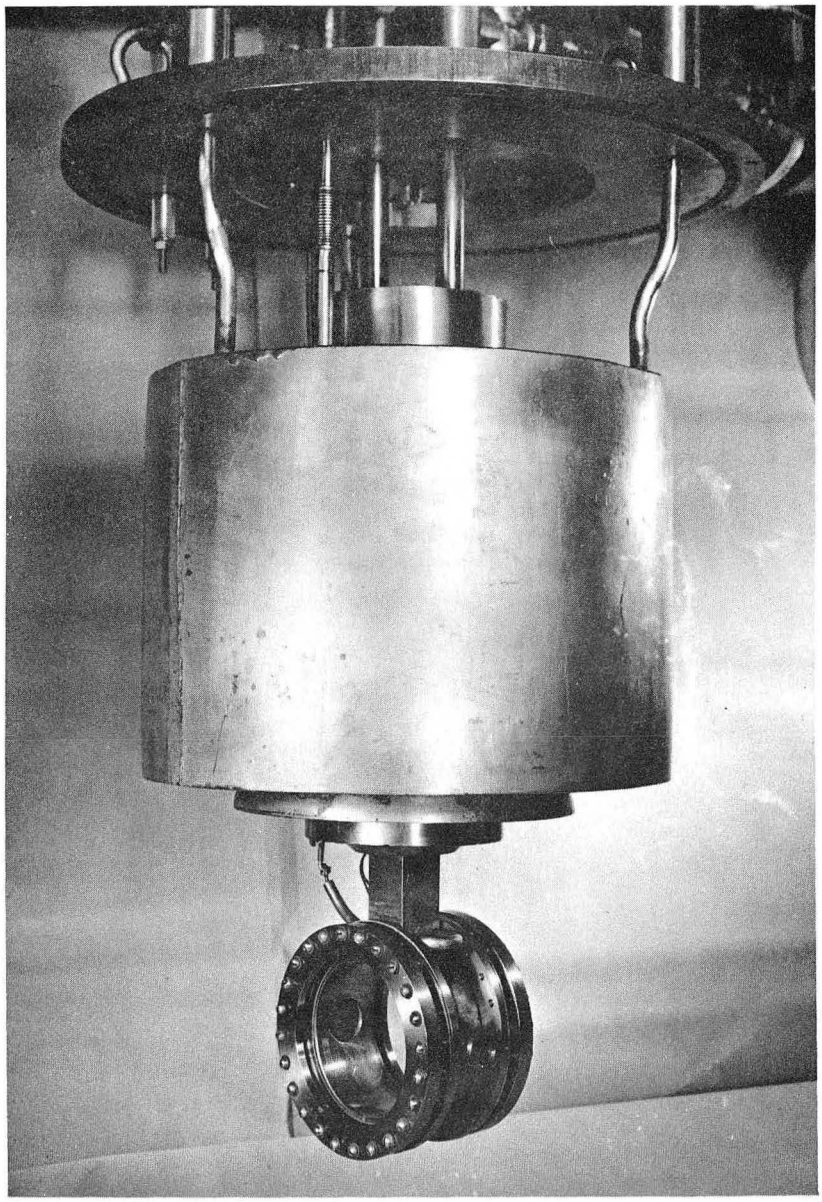

ZN-2100

Fig. 2.

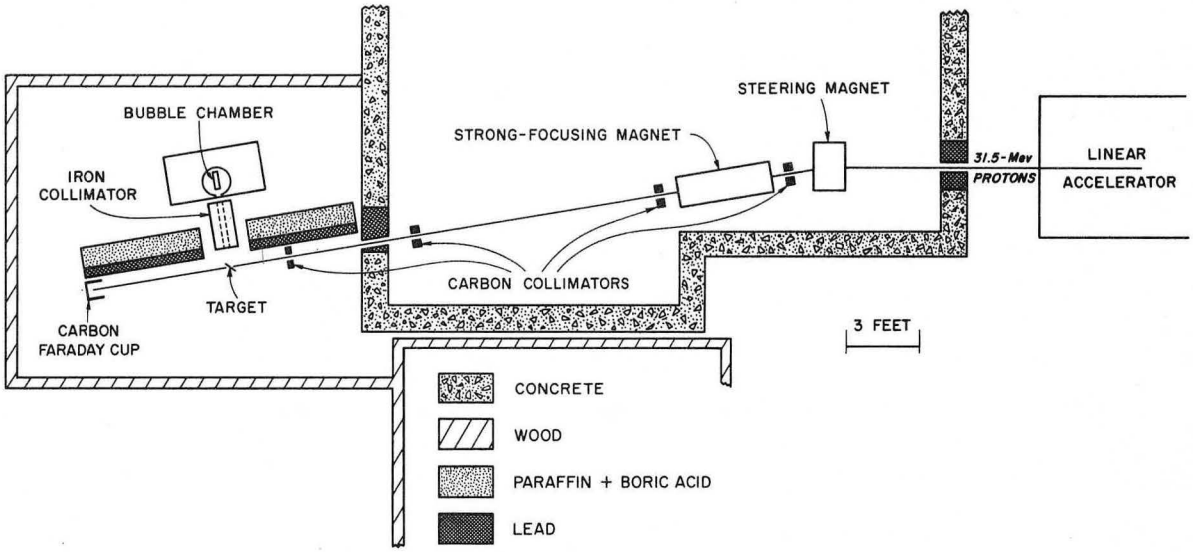
BUBBLE CHAMBER
IRON COLLIMATOR
TARGET
CARBON FARADAY CUP
STRONG-FOCUSING MAGNET
STEERING MAGNET
31.5-Mev PROTONS
LINEAR ACCELERATOR
CARBON COLLIMATORS
3 FEET
CONCRETE
WOOD
PARAFFIN + BORIC ACID
LEAD
MU-14903

Fig. 3.

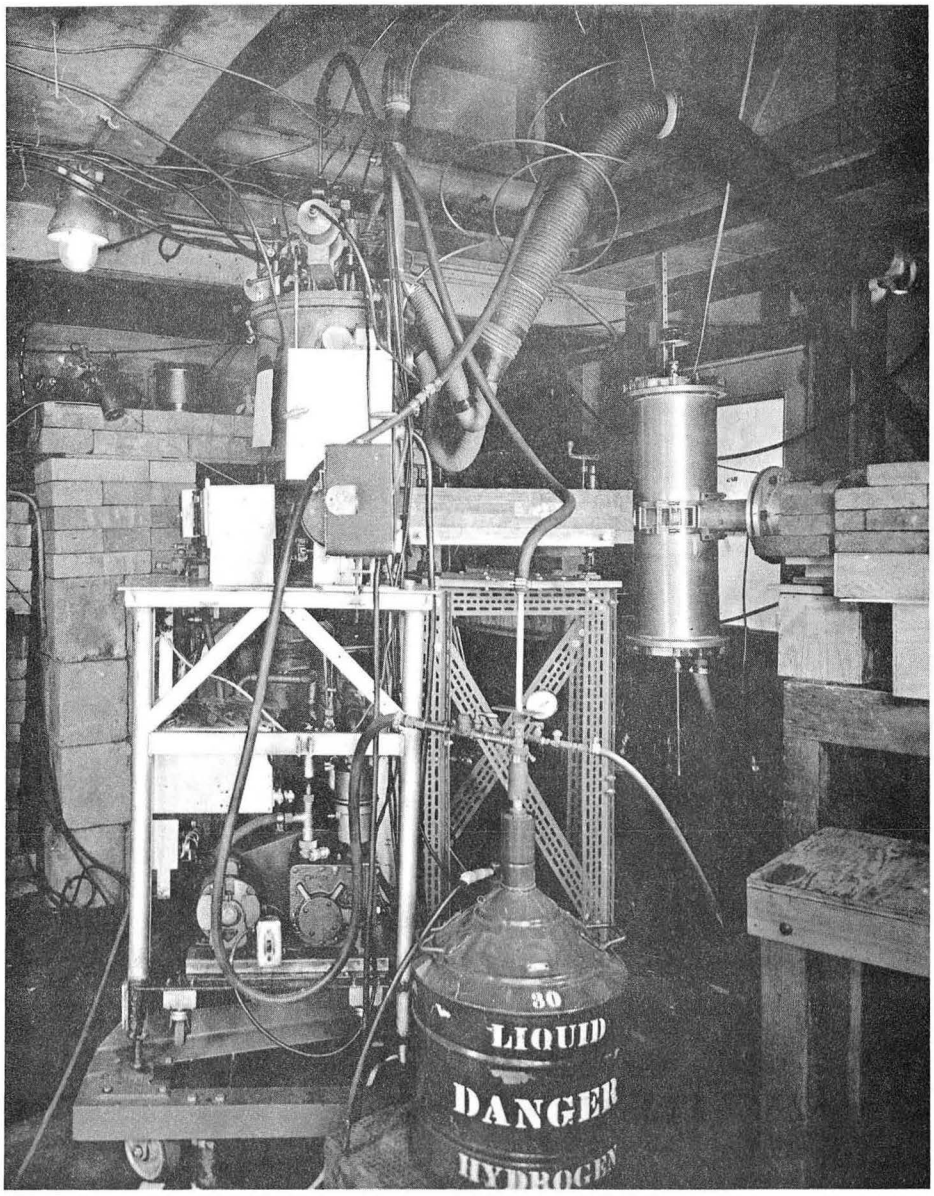

ZN-2049

Fig. 4.

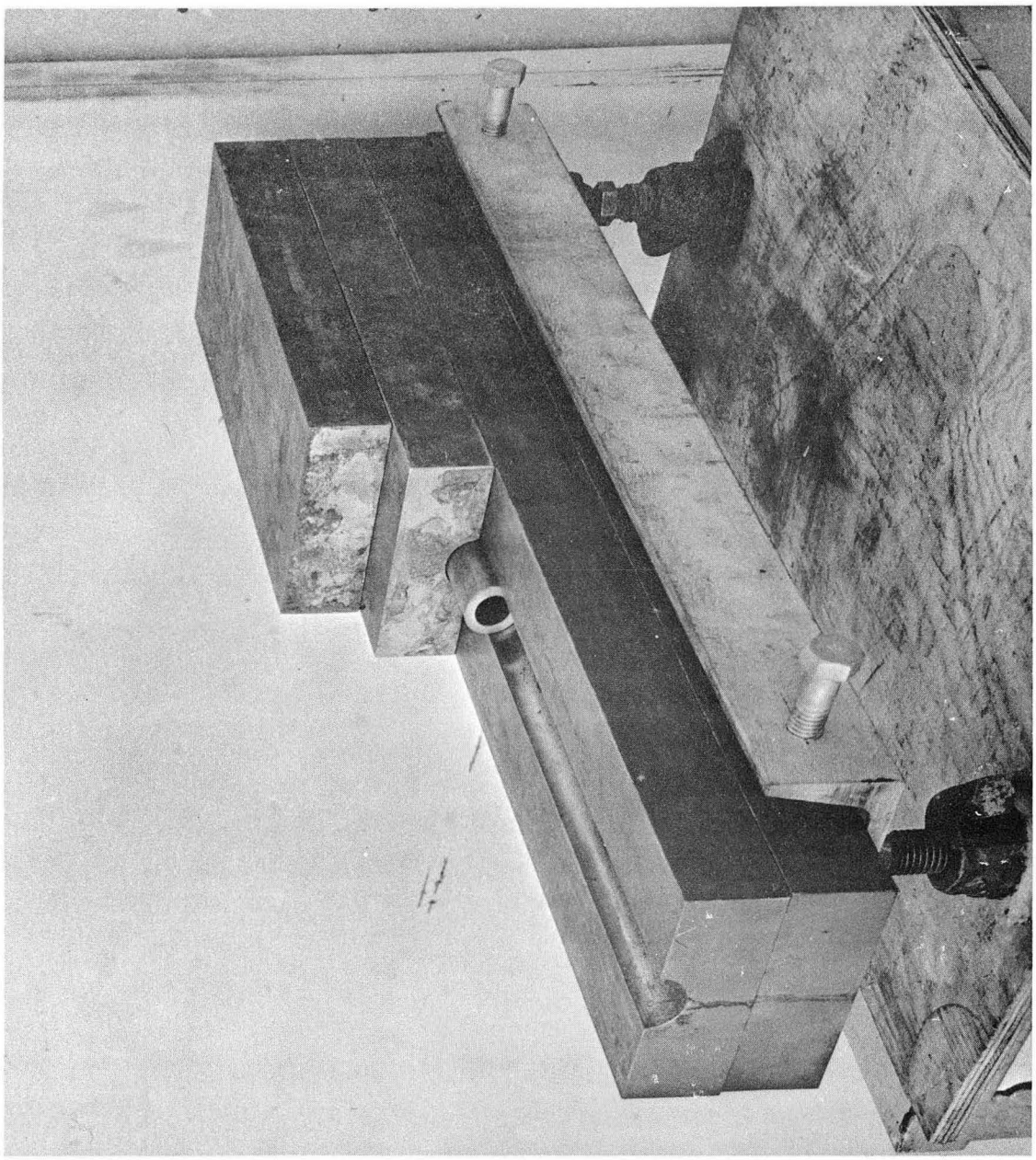

ZN-2050

Fig. 5.

ZN-2052

Fig. 6.

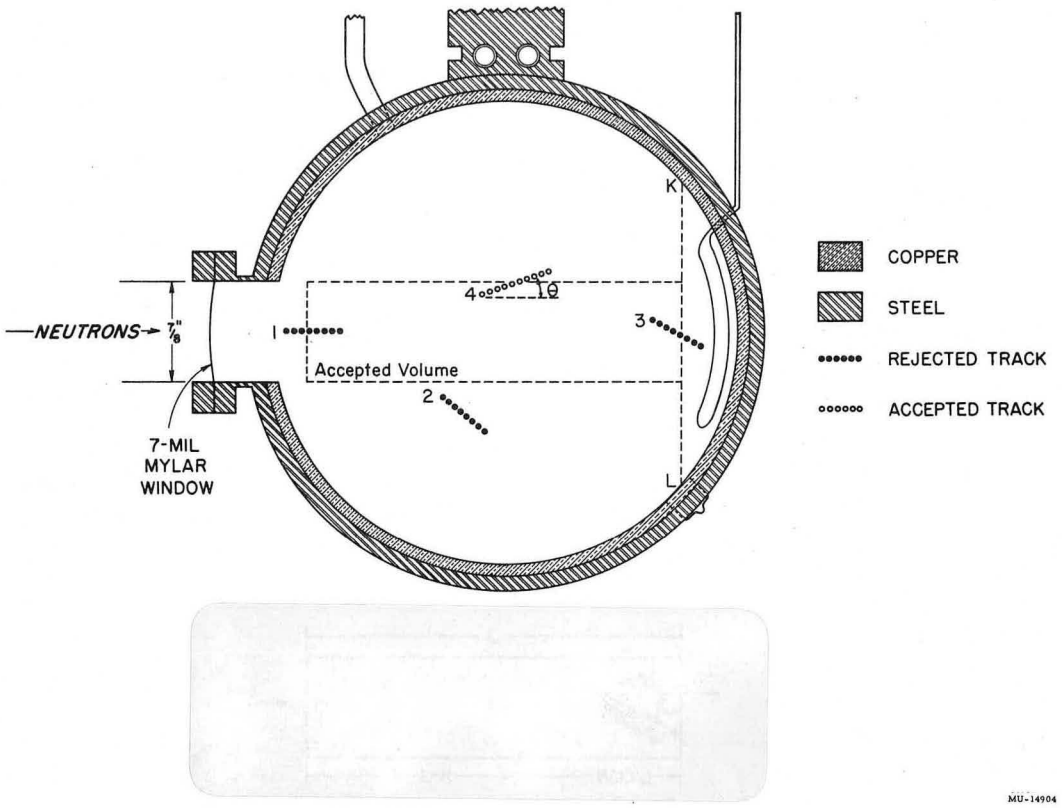
NEUTRONS
7/8"
7-MIL
MYLAR
WINDOW
Accepted Volume
1
2
3
4
5
K
L
COPPER
STEEL
REJECTED TRACK
ACCEPTED TRACK
MU-14904

Fig. 7.

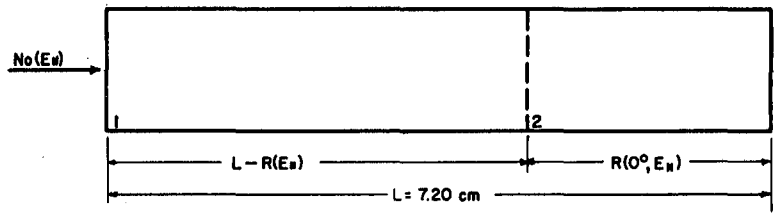

Figure A

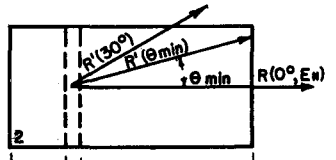

Figure B

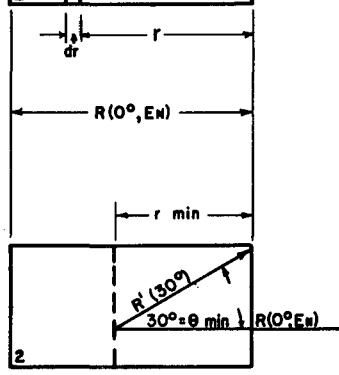

Figure C

MU-16519

Fig. 8.

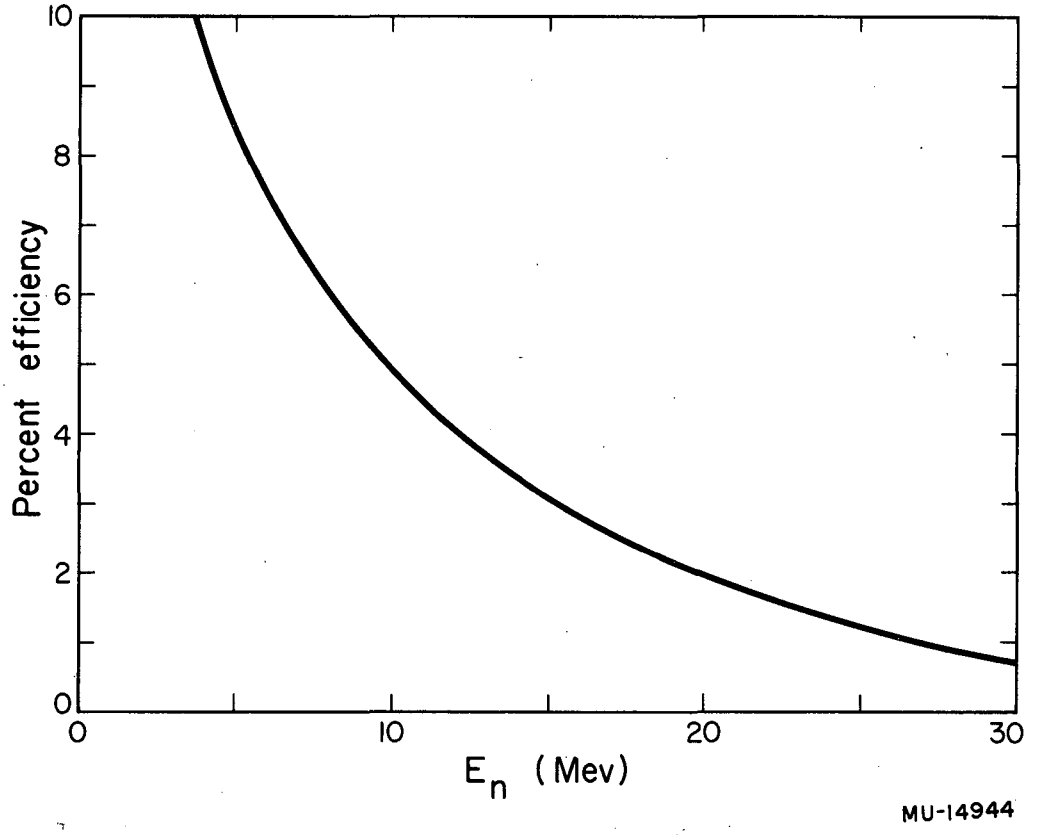

Fig. 9.

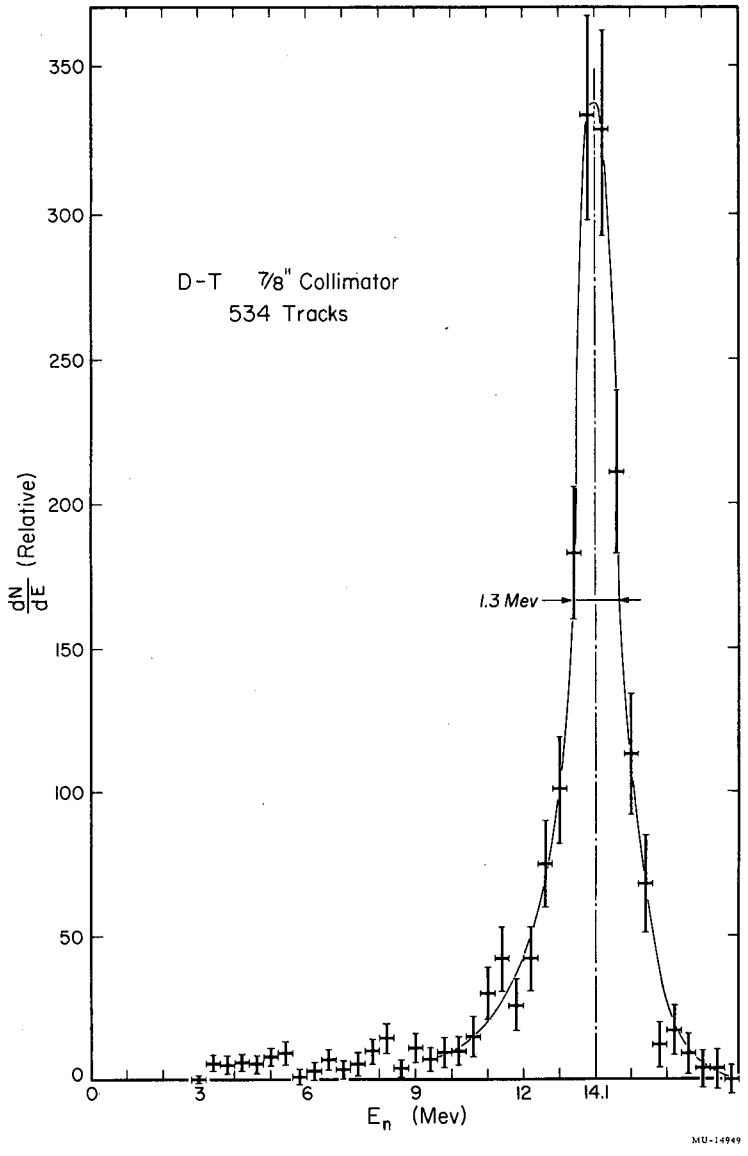
D-T 7/8" Collimator
534 Tracks
1.3 Mev
dN/dE (Relative)
E_n (Mev)
0
3
6
9
12
14.1
50
100
150
200
250
300
350
MU-14949

Fig. 10.

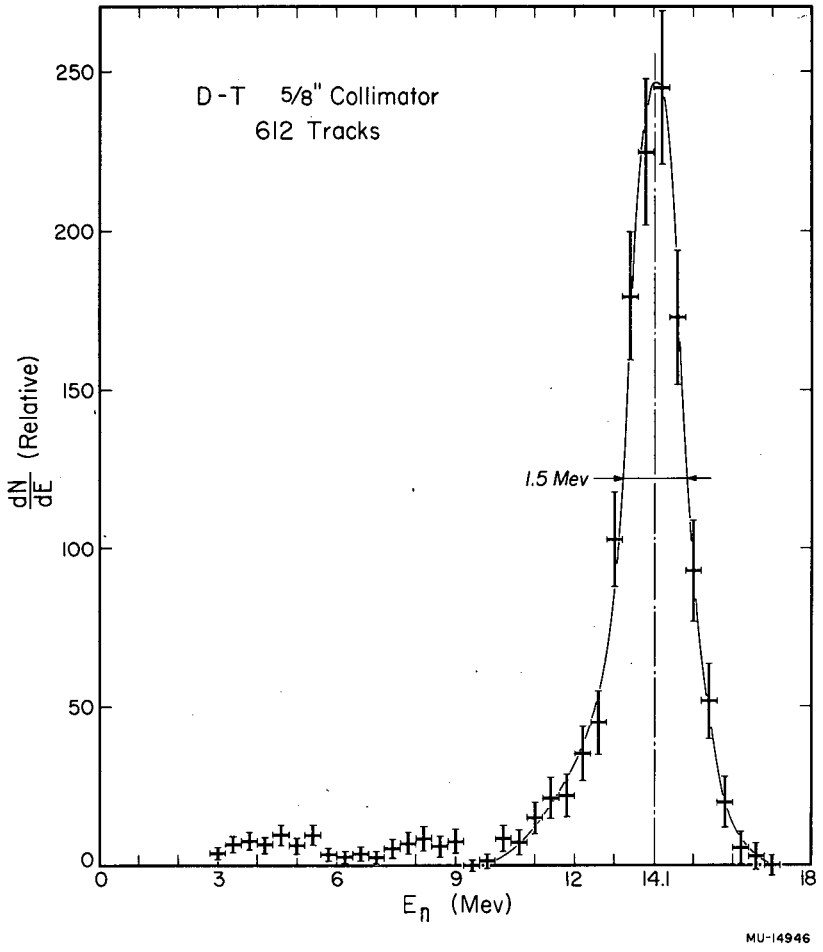
D-T 5/8" Collimator
612 Tracks
1.5 Mev
dN/dE (Relative)
250
200
150
100
50
0
0
3
6
9
12
14.1
18
E_n (Mev)
MU-14946

Fig. 11.

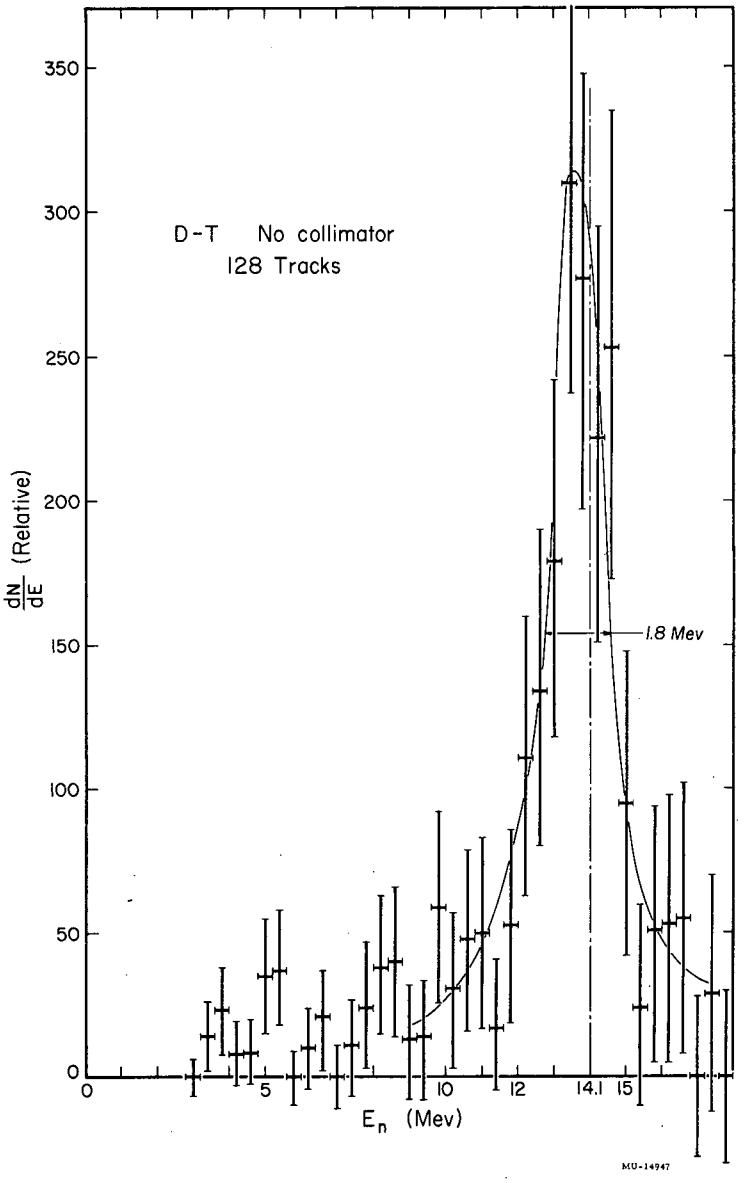
D-T No collimator
128 Tracks
1.8 Mev
dN/dE (Relative)
E_n (Mev)
0
50
100
150
200
250
300
350
5
10
12
14.1
15
MU-14947

Fig. 12.

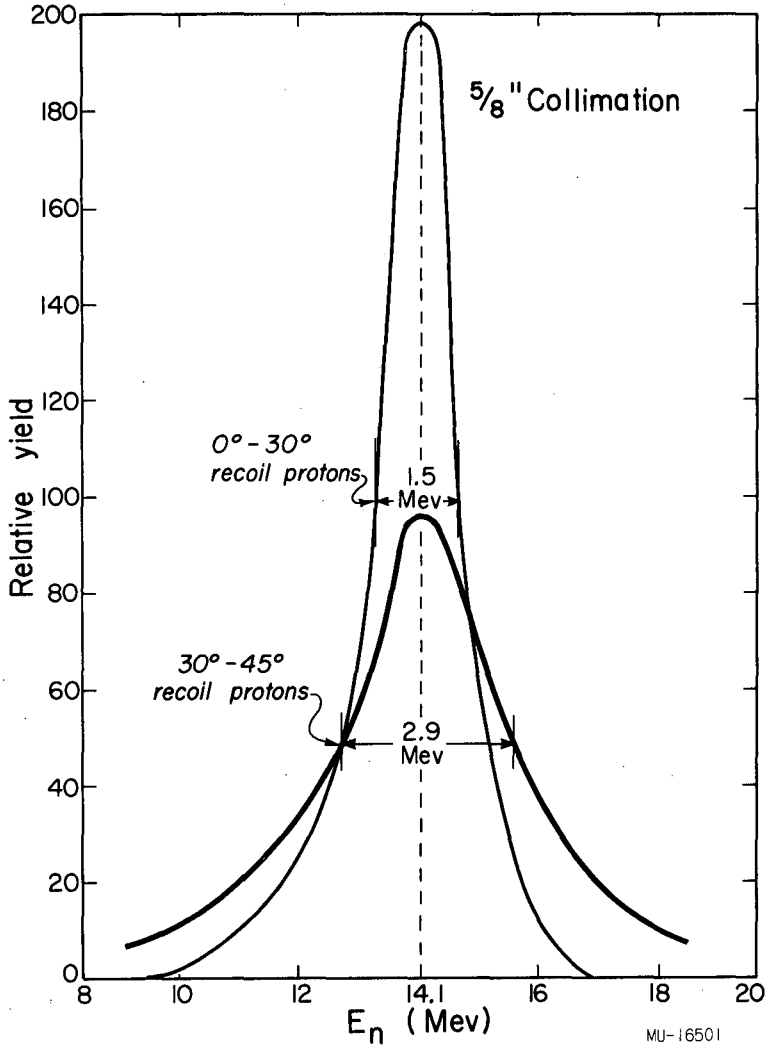
5/8" Collimation
0°-30°
recoil protons
1.5
Mev
30°-45°
recoil protons
2.9
Mev
Relative yield
200
180
160
140
120
100
80
60
40
20
0
8
10
12
14.1
16
18
20
En (Mev)
MU-16501

Fig. 13.

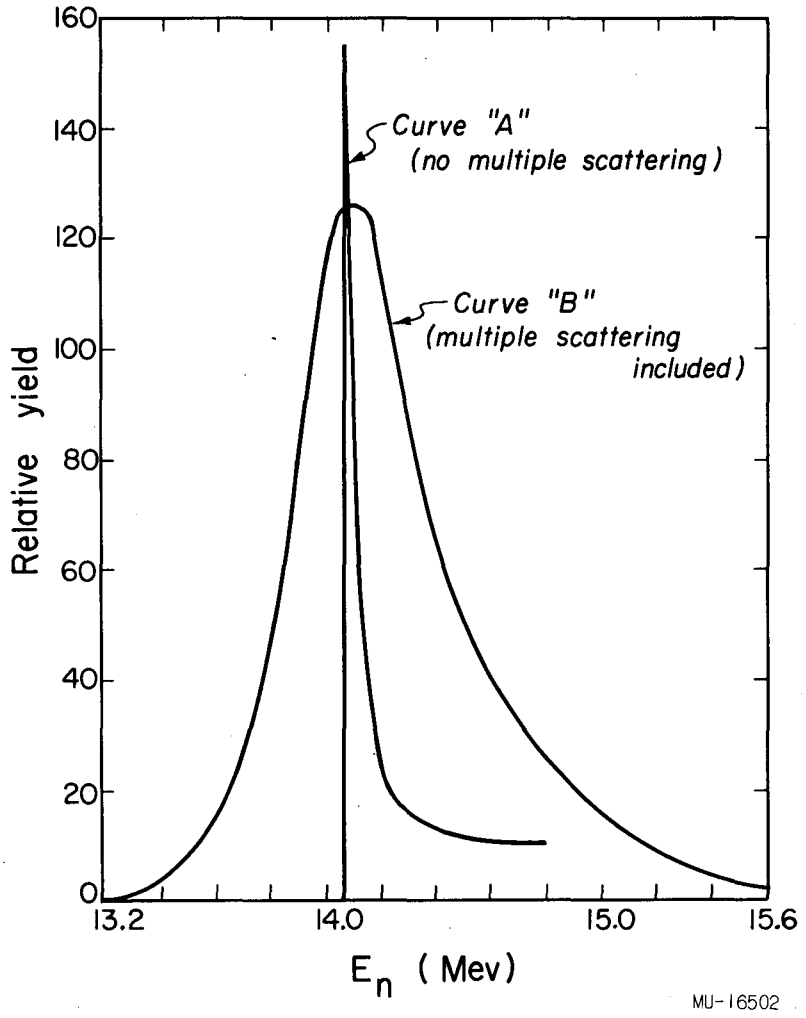
160
140
120
100
80
60
40
20
0
Relative yield
Curve "A"
(no multiple scattering)
Curve "B"
(multiple scattering
included)
13.2
14.0
15.0
15.6
E_n (Mev)
MU-16502

Fig. 14.

UCRL

UNIVERSITY OF CALIFORNIA

Radiation Laboratory

BERKELEY, CALIFORNIA